Comparison of Three Voltage Saturation Algorithms in Shunt Active Power Filters with Selective Harmonic Control

IEEE TRANSACTIONS ON INDUSTRY APPLICATIONS 2019-IPCC-1174

Comparison of Three Voltage Saturation Algorithms in Shunt Active Power Filters with Selective Harmonic Control

Albino Amerise, Michele Mengoni, *Member*, *IEEE*, Gabriele Rizzoli, Luca Zarri, *Senior Member*, *IEEE*, Angelo Tani, and Domenico Casadei, *Fellow*, *IEEE*

***Abstract*— An array of proportional-resonant regulators is often used in shunt active power filters to control the grid currents and reduce the harmonic distortion caused by a distorting load. The voltage that is necessary to compensate for the current harmonics must be consistent with the available dc-link voltage. In this paper, three adaptive algorithms for the exploitation of the dc-link voltage are developed and compared. These algorithms adaptively change the voltage saturation of each regulator to preserve the control capability of the fundamental component of the current when the available voltage is not enough to control the filter current. Simultaneously, they try to improve the quality of the grid current because the dc-link voltage of the active power filter is allocated to the regulators to compensate only the most significant harmonics. Some experimental results are shown to demonstrate the feasibility of the three algorithms.**

Keywords*— *Active power filter, resonant regulators, voltage saturation, anti-windup, current quality

I. Introduction

Nonlinear loads, such as ac/dc rectifiers, cause undesirable phenomena in the operation of power systems, such as harmonic pollution and a reduction of the power factor. Power Conditioning Systems (PCS) can be used to compensate for these disturbances and to improve the quality of the grid currents and voltages.

Shunt Active Power Filters (APFs) fall into this category of devices. As shown in Fig. 1, they are connected through a decoupling inductance to the Point of Common Coupling (PCC), the point of interconnection of the power supply network, and multiple loads. APFs are used to adjust the grid power factor and to compensate grid harmonic currents [1].

Several approaches have been investigated and tested for the current control loop, which usually has to track a reference signal composed of several harmonic components. Proportional-integral controllers implemented in a reference frame rotating at the frequency of the disturbing harmonics can be used [2]-[4]. Dead-beat and hysteresis controllers [5]-[7] require less computational effort than PI controllers implemented in rotating reference frames, but they are not so effective in compensating the harmonic distortion. Recently, repetitive control has been proposed due to its excellent performance in terms of harmonic compensation and low computational burden [8], but it requires an accurate analysis of stability and cannot be used for selective elimination of the harmonics. Another solution that has proven its value in recent years is the use of resonant controllers implemented in the stationary reference frame, or in rotating reference frames, to cancel more harmonic components of the grid current at a time [9]-[11]. In [12], several kinds of resonant controllers are compared, such as multiple rotating integrators, stationary frame resonant controllers, proportional-sinusoidal signal integrators, and vector PI controllers, to determine, for each method, the operating frequency range, and the stability limit.

Resonant controllers in the stationary reference frame do not need time-expensive calculations for the direct and inverse transformation of the reference frame. The efficiency in harmonic compensation is similar to that of repetitive controllers, but an array of resonant controllers allows adjusting the current harmonics selectively because each regulator is approximately independent of the others [13].

The primary constraint of an APF is the dc-link voltage, whose low value may affect the stability of the system. As the output voltage of an APF is composed of contributions at different frequencies, a single prevailing harmonic may cause

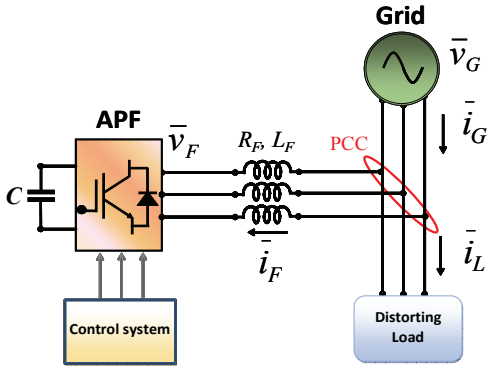

Fig.1. Scheme of a shunt active power filter.

Manuscript received September 13, 2019; revised December 31, 2019; accepted January 29, 2020. A. Amerise, M. Mengoni, G. Rizzoli, L. Zarri, A. Tani, and D. Casadei are with the Department of Electric, Electronic and Information Engineering "G. Marconi", University of Bologna, Bologna, 40136 Italy (albino.amerise2@unibo.it, michele.mengoni@unibo.it, gabriele.rizzoli@unibo.it, luca.zarri2@unibo.it, angelo.tani@unibo.it, domenico.casadei@unibo.it).

the total voltage to exceed the voltage limit resulting from the available dc voltage. To preserve the fundamental component of the output voltage, which is responsible for the control of the average value of the dc-link voltage, a strategy that allocates the available dc-link voltage among the regulators must be developed [14]. This issue is linked to a similar problem, which has been investigated in recent years, i.e., the problem of distortion-free saturators for grid-tied converters under unbalanced conditions. Typically, the control system of a grid-tied converter includes a saturator block that limits the magnitude of the current/voltage reference vector but keeps its original phase. Unfortunately, this strategy may cause low-order harmonics if the reference vectors move on an elliptical trajectory (unbalanced conditions). To reduce the distortion of the saturated signals, the reference vector can be multiplied by a scale factor to adapt the elliptical trajectory over a period to the limit voltage circle [15]. Preventing voltage distortion in multifrequency current control during saturated operation is recognized as a difficult problem. In [16]-[17], the principle of realizable references is used to design a distortion-free control algorithm. When the converter operates in saturated conditions, the converter-current references are recalculated such that the set-points return into the linear range.

Differently from those researches, in this paper, focused on APFs, the distortion of the output voltage is assumed unavoidable to cancel the current harmonics of a nonlinear load. This paper improves the results presented in [18] and compares some saturation algorithms of the output voltage of an array of resonant regulators for the current loop of an APF. These algorithms define an independent limit for each voltage harmonic so that the saturation of one of them does not affect the control of the remaining ones. The voltage limits are dynamically changed depending on the operating conditions in such a way that the regulators that require a high voltage can exploit a higher fraction of the available dc-link voltage.

II. Mathematical Model of a Shunt APF

A. Operation Principles of a Shunt APF

The operation of an APF must be consistent with the available voltage across the floating capacitor C. The voltage E_F of the dc link depends on the electrostatic energy stored in the capacitor, whose rate of change is related to the instantaneous active power of the converter. If the losses of the APF are neglected, the following expressions can be written:

$$\frac{d}{dt}\left(\frac{1}{2}CE_F^2\right) = P_F \tag{1}$$

$$P_F = \frac{3}{2}\bar{v}_F \cdot \bar{i}_F \tag{2}$$

where P_F is the instantaneous active power at the input of the APF, $\bar{v}_F$ and $\bar{i}_F$ are respectively the output voltage and current vectors of the APF, and "·" is the dot product operator, defined as the sum of the products of the corresponding components of the two vectors.

To control the filter current, it is necessary to find the relationship between $\bar{v}_F$ and $\bar{i}_F$. In a reference frame aligned with the grid voltage $\bar{v}_G$, this relationship is given by the equation of the decoupling inductance:

$$\bar{v}_G = R_F\bar{i}_F + j\omega L_F\bar{i}_F + L_F\frac{d\bar{i}_F}{dt} + \bar{v}_F \tag{3}$$

where $\bar{v}_G$ is the grid voltage, R_F and L_F are respectively the filter resistance and inductance, and ω is the fundamental grid frequency.

It is straightforward from (3) to find the expression of the instantaneous active power P_G exchanged between the grid and the APF:

$$P_G = \frac{3}{2}R_F i_F^2 + \frac{d}{dt}\left(\frac{3}{4}L_F\left|\bar{i}_F\right|^2\right) + P_F \tag{4}$$

where

$$P_G = \frac{3}{2}\bar{v}_G \cdot \bar{i}_F = \frac{3}{2}v_G i_{Fd} \tag{5}$$

In (5), i_{Fd} is the d-axis component of the filter current $\bar{i}_F$, and v_G is the magnitude of the grid voltage $\bar{v}_G$.

Equation (4), combined with (1), can be rewritten to emphasize the derivative of the total electromagnetic energy of the system.

$$\frac{d}{dt}\left(\frac{1}{2}CE_F^2 + \frac{3}{4}L_F\left|\bar{i}_F\right|^2\right) = P_G - \frac{3}{2}R_F\left|\bar{i}_F\right|^2. \tag{6}$$

If the Joule losses of the filter resistance are negligible, (6) shows that the rate of change of the energy stored in the reactive elements of the system depends on the instantaneous active power P_G, which is proportional to i_{Fd}. Therefore, the voltage level of the dc-link capacitor can be indirectly controlled by adjusting the total energy of the system through i_{Fd}, under the assumption that the magnetic energy of the filter inductance is regarded as a measurable disturbance, which can be appropriately counterbalanced.

To find the relationship between the values Q_G and Q_F of the reactive power exchanged respectively by the power grid and the APF, one can calculate the dot product between each side of (3) and $j\frac{3}{2}\bar{i}_F$.

$$Q_G = \frac{3}{2}\omega L_F\left|\bar{i}_F\right|^2 + Q_F. \tag{7}$$

where Q_G can be explicitly written as follows:

$$Q_G = -\frac{3}{2}v_G i_{Fq}. \tag{8}$$

Equations (7) and (8) show that it is possible to control the reactive power injected into the grid by the APF by acting on the q-component of the filter current i_{Fq} and compensating for the reactive power of the decoupling inductance.

With reference to Fig. 1, where $\bar{i}_L$ and $\bar{i}_G$ denote the load and grid current vectors, the balance of the currents at the PCC leads to the following equation:

$$\bar{i}_F = \bar{i}_G - \bar{i}_L \,. \tag{9}$$

If the high-frequency components, identified by the subscript "HF", are considered, (10) allows finding the harmonic content of $\bar{i}_F$ that nullifies $\bar{i}_{G,HF}$:

$$\bar{i}_{F,HF,ref} = -\bar{i}_{L,HF} \,. \tag{10}$$

Equation (10) states that the shunt APF has to generate the high-frequency components of the load current to relieve the grid from providing the undesired harmonics.

Since the energy carried by the high-frequency harmonics of the voltages and currents is usually much lower than that of the fundamental components, it results that the low-frequency components of the i_{Fd} and i_{Fq} can be used to control the average energy of the capacitor and the reactive power at the PCC, according to (5) and (8). Conversely, the high-frequency components of $\bar{i}_F$ can be controlled to compensate for the distorting currents of load, according to (10).

B. Array of Resonant Controllers

The setpoint $\bar{i}_{F,HF,ref}$ is composed of several harmonic components. To make the output current closely track the reference input, a specific proportional-resonant regulator can be used for each harmonic. Equations (9) and (10) show that the high-frequency term of the error signal at the input of the array of proportional-resonant controllers is:

$$\bar{i}_{F,HF,ref} - \bar{i}_{F,HF} = -\bar{i}_{G,HF} \,. \tag{11}$$

Thus, if $R_k(s)$ is the transfer function of the kth proportional-resonant controller in the stationary reference frame and $\bar{v}^S_{Fk,req}$ is its output voltage, the following expression can be written:

$$\bar{v}^S_{Fk,req} = R_k(s)(-\bar{i}^S_{G,HF}) \tag{12}$$

where the superscript S means that the variables are written in the stationary reference frame.

The transfer function of R_k is as follows [19]:

$$R_k(s) = K_{P,k} + 2K_{I,k}\frac{s\cos\theta_k + \omega_{cr,k} - \omega_k \sin\theta_k}{s^2 + 2\omega_{cr,k}s + \omega^2_{cr,k} + \omega^2_k} \tag{13}$$

where ω_k is the angular frequency of the disturbance, $K_{P,k}$ and $K_{I,k}$ are the proportional and resonant gains, $\omega_{cr,k}$ and θ_k are parameters related to the sharpness of the resonance and the phase angle at the resonance frequency.

III. Saturation Strategies

The rated current $I_{F,max}$ of the converter and the available voltage E_F of the dc-link limit the performance of an APF. These constraints can be expressed by the following inequalities:

$$\left|\bar{i}_F\right| \le I_{F,max} \,. \tag{14}$$

$$\left|\bar{v}_F\right| \le V_{F,max} \,. \tag{15}$$

where $V_{F,max}$ is equal to $0.577E_F$ if space vector modulation is used.

The output voltage vector of the APF is the sum of the outputs of the resonant controllers and can be written as follows:

$$\bar{v}^S_{F,ref} = \sum_{k=1,..,n} \bar{v}^S_{Fk,ref} \tag{16}$$

where $\bar{v}^S_{Fk,ref}$ (k=1, …, n) is the contribution to the output voltage produced by the kth regulator.

The output voltage given by (16) must comply with (15), so the kth regulator can exploit only a fraction of the available dc-link voltage. Consequently, the output voltage of each proportional-resonant regulator is constrained by a saturation block, whose equation can be written as follows:

$$\bar{v}^S_{Fk,ref} = c_k \bar{v}^S_{Fk,req} \;\; (k = 1,\ldots, n) \tag{17}$$

where c_k is a positive coefficient not greater than one ($c_k \le 1$), and $\bar{v}^S_{Fk,req}$ is the voltage requested by the kth resonant controller without saturation constraints. The block diagram of the array of resonant controllers is shown in Fig. 2. To avoid the windup of the regulators, it is necessary to implement an anti-windup strategy, which may be a feedback signal to the input with a back-calculation gain, or recalculation of the error at the input of the regulator. This latter technique seems to be more practical in digital applications [14].

The allocation of the dc-link voltage to the regulators should privilege the control of the fundamental component of the filter current, which directly affects the stability of the capacitor voltage. In contrast, the residual voltage that is not used to control the fundamental component can be utilized to compensate for the harmonic currents. As a consequence, the coefficient c_1, which is related to the fundamental component of the filter voltage, is usually equal to 1, provided that the voltage magnitude of $\bar{v}_{F1,ref}$ is below $V_{F,\max}$. Conversely, the other coefficients c_k may be lower than 1, depending on whether the available dc-link voltage is sufficient or not to synthesize the resulting total voltage $\bar{v}^S_{F,ref}$. Different strategies can be used for the repartition of the available voltage among the regulators and for the selection of the coefficients c_k. Three different strategies are considered hereafter.

A. Strategy 1

According to this strategy, coefficients c_k (k = 2, …, n) are assumed equal to each other. This constant value c can be determined by calculating the constant that satisfies inequality (18), obtained by applying the triangular inequality to (16), and considering (15) and (17):

This article has been accepted for publication in a future issue of this journal, but has not been fully edited. Content may change prior to final publication. Citation information: DOI 10.1109/TIA.2020.2972853, IEEE Transactions on Industry Applications

$$\left|\bar{v}^S_{F1,ref}+\sum_{k=2,\dots,n}\bar{v}^S_{Fk,ref}\right|\le\left|\bar{v}^S_{F1,ref}\right|+\sum_{k=2,\dots,n}\left|\bar{v}^S_{Fk,ref}\right|\le$$
$$\le\left|\bar{v}^S_{F1,ref}\right|+c\sum_{k=2,\dots,n}\left|\bar{v}^S_{Fk,req}\right|\le V_{F,\max} \quad (18)$$

The maximum admissible value for c is

$$c=\frac{V_{F,\max}-\left|\bar{v}^S_{F1,ref}\right|}{\sum_{k=2,\dots,n}\left|\bar{v}^S_{Fk,req}\right|}. \quad (19)$$

According to strategy 1, c is constant at steady state because it depends only on the magnitude of the voltage vectors $\bar{v}^S_{Fk,req}$ and $\bar{v}^S_{F1,ref}$.

The total voltage $\bar{v}^S_{F,req}$ requested by the array of regulators is composed of several contributions $\bar{v}^S_{Fk,req}$ at different frequencies. Its magnitude is not constant over a fundamental period and can be instantaneously lower or higher than the voltage limit $V_{F,max}$. However, strategy 1 considers the worst case and assumes that the vector components of the output voltage add up with the same phase angle. Since the magnitude of the voltage harmonics is bounded on the basis of this unlikely condition, the exploitation of the dc-link may be suboptimal.

B. Strategy 2

Coefficients c_k (k = 2, …, n) are assumed equal to each other, as in strategy 1. Let us call this common value c'. This quantity differs from c, defined for strategy 1 because it is calculated without the simplification introduced by the triangular inequality. Substituting (16)-(17) in (15), and considering c_k=c', leads to the following inequality:

$$\left|\bar{v}^S_{F1,ref}+\sum_{k=2,\dots,n}\bar{v}^S_{Fk,ref}\right|=\left|\bar{v}^S_{F1,ref}+c'\sum_{k=2,\dots,n}\bar{v}^S_{Fk,req}\right|\le V_{F,\max} \quad (20)$$

Squaring both sides, one obtains:

$$a_2(c')^2+2a_1c'+a_0\le 0 \quad (21)$$

where a_0, a_1, and a_2 are defined as follows:

$$a_0=\left|\bar{v}^S_{F1,ref}\right|^2-V^2_{F,\max} \quad (22)$$

$$a_1=\bar{v}^S_{F1,ref}\cdot\sum_{k=2,\dots,n}\bar{v}^S_{Fk,req} \quad (23)$$

$$a_2=\left|\sum_{k=2,\dots,n}\bar{v}^S_{Fk,req}\right|^2. \quad (24)$$

Inequality (21) admits an interval of solutions for c' if its discriminant is positive, as shown in (25).

$$\left(\bar{v}^S_{F1,ref}\cdot\sum_{k=2,\dots,n}\bar{v}^S_{Fk,req}\right)^2+\left[V^2_{F,\max}-\left(\bar{v}^S_{F1,ref}\right)^2\right]\left|\sum_{k=2,\dots,n}\bar{v}^S_{Fk,req}\right|^2\ge 0. \quad (25)$$

A sufficient condition to satisfy (25) is that $\left|\bar{v}^S_{F1,ref}\right|$ is lower than $V_{F,\max}$. The maximum value of c' that satisfies (21) is

$$c'=\frac{\sqrt{a_1^2-a_2a_0}-a_1}{a_2} \quad (26)$$

where the denominator a_2 is usually a positive number different from zero.

It is worth noting that c' is a time-variant quantity because coefficients a_1 and a_2 depend on the phase angle of the voltage vectors $\bar{v}^S_{Fk,req}$ (k=2, …, n), as can be seen from (23)-(24). Even at a steady state, the saturation boundary of the regulators may fluctuate to maximize the range of the output voltage.

C. Strategy 3

During a fundamental period, some harmonic components $\bar{v}^S_{Fk,req}$ increase the magnitude of the total output voltage, while others decrease it depending on their phase angle. This latter group of harmonics should not be limited since they usefully contribute to reducing the total output voltage requested. These harmonics can be found by evaluating the derivative of the magnitude of total output voltage with respect to the magnitude of each voltage harmonic:

$$\frac{\partial}{\partial\left|\bar{v}^S_{Fk,req}\right|}\left|\bar{v}^S_{F,req}\right|=\frac{\partial}{\partial\left|\bar{v}^S_{Fk,req}\right|}\left|\bar{v}^S_{F1,ref}+\sum_{h=2,\dots,n}\bar{v}^S_{Fh,req}\right|. \quad (27)$$

Alternatively, considering the derivative of $\left|\bar{v}^S_{F,req}\right|$ squared is numerically simpler. One finds the following expression:

$$\frac{\partial}{\partial\left|\bar{v}^S_{Fk,req}\right|}\left|\bar{v}^S_{F,req}\right|^2=\frac{\partial}{\partial\left|\bar{v}^S_{Fk,req}\right|}\left|\bar{v}^S_{F1,ref}+\sum_{h=2,\dots,n}\bar{v}^S_{Fh,req}\right|^2=$$
$$=\frac{\partial}{\partial\left|\bar{v}^S_{Fk,req}\right|}\left(\left|\bar{v}^S_{F1,ref}\right|^2+2\bar{v}^S_{F1,ref}\cdot\sum_{h=2,\dots,n}\bar{v}^S_{Fh,req}+\left|\sum_{h=2,\dots,n}\bar{v}^S_{Fh,req}\right|^2\right)=$$
$$=2\left|\bar{v}^S_{F1,ref}\right|\cos\psi_k+2\left|\bar{v}^S_{Fk,req}\right|+2\sum_{h>1,h\ne k}\left|\bar{v}^S_{Fh,req}\right|\cos\psi_{hk}. \quad (28)$$

where ψ_k represents the relative phase of the kth harmonic with respect to the fundamental one, and ψ_{hk} is the phase difference of the kth and hth harmonics.

If the magnitude of the voltage harmonics is negligible compared to the fundamental component, one finds:

$$\frac{\partial}{\partial\left|\bar{v}^S_{Fk,req}\right|}\left|\bar{v}^S_{F,ref}\right|^2\cong 2\left|\bar{v}^S_{F1,ref}\right|\cos\psi_k \quad (29)$$

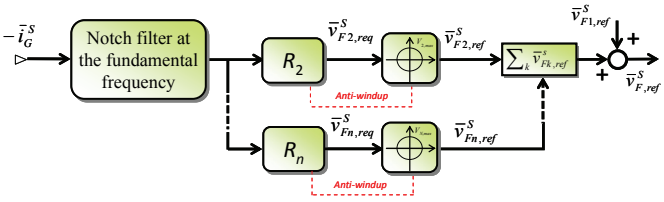

Fig.2. Structure of the array of proportional resonant regulators with anti-windup.

This article has been accepted for publication in a future issue of this journal, but has not been fully edited. Content may change prior to final publication. Citation information: DOI 10.1109/TIA.2020.2972853, IEEE Transactions on Industry Applications

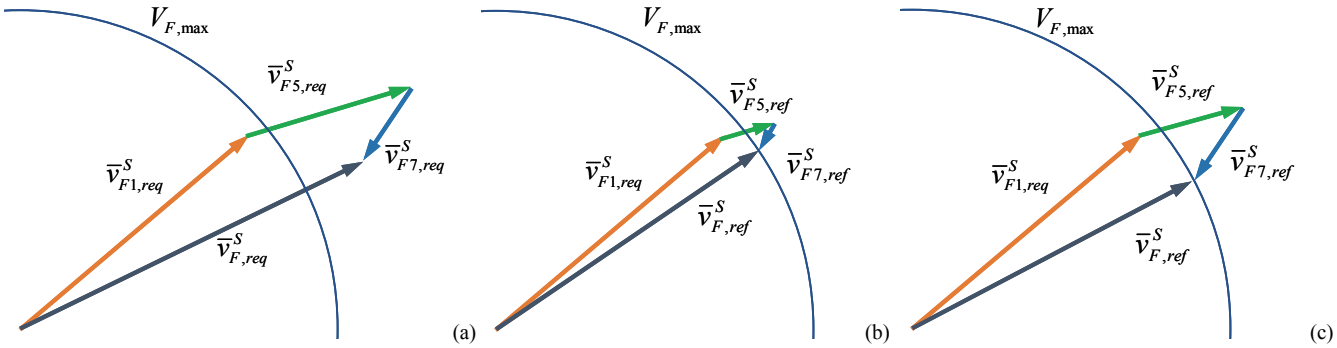

Fig.3. Representation of the space voltage vectors when the magnitude of the total voltage exceeds the maximum voltage. Requested output voltage vectors (a). Output voltage vectors with strategy 2 (b). Output voltage vectors with strategy 3 (c).

Equations (28) and (29) express how the magnitude of the output voltage vector of the converter, $\bar{v}^S_{F,ref}$, depends on the magnitude of the single harmonics. In particular, (29) reveals that if the magnitude of the kth voltage harmonic increases, the magnitude of the output voltage vector does not increase necessarily, but its variation is related to the angle ψ_k.

The harmonics with a negative derivative resulting from (29) do not need to be saturated. Let us call N_n the set of indexes of the vectors that give a negative or null contribution to the magnitude of the output voltage, and N_p the set of the indexes of the vectors that give a positive contribution.

The coefficient c_k is assumed to be equal to 1 if $k \in N_n$. For the remaining vectors ($k \in N_p$), c_k is assumed to be the maximum value of c'' that verifies the following inequality:

$$\left| \bar{v}^S_{F1,ref} + \sum_{k \in N_n} \bar{v}^S_{Fk,req} + c'' \sum_{k \in N_p} \bar{v}^S_{Fk,req} \right| \le V_{F,\max} . \qquad (30)$$

Using the same procedure adopted for strategy 2, one can calculate the explicit expression of c", which is as follows:

$$c'' = \frac{\sqrt{b_1^2 - b_2 b_0} - b_1}{b_2} \qquad (31)$$

where

$$b_0 = \left| \bar{v}^S_{F1,ref} + \sum_{k \in N_n} \bar{v}^S_{Fk,req} \right|^2 - V^2_{F,\max} \qquad (32)$$

$$b_1 = 2 \left(\bar{v}^S_{F1,ref} + \sum_{k \in N_n} \bar{v}^S_{Fk,req} \right) \cdot \sum_{k \in N_p} \bar{v}^S_{Fk,req} \qquad (33)$$

$$b_2 = \left| \sum_{k \in N_p} \bar{v}^S_{Fk,req} \right|^2 \qquad (34)$$

The coefficient c" can be found if the discriminant $b_1^2 - b_2 b_0$ in (31) is positive or zero, and the denominator b_2 is different from zero. The former condition is verified if $\left|\bar{v}^S_{F1,ref}\right|$ is lower than $V_{F,\max}$, the latter is verified because all the vectors with $k \in N_p$ have a positive-sequence component in the direction of $\bar{v}^S_{F1,ref}$, since $\cos\psi_k > 0$ for all of them.

A graphical analysis can be useful to highlight the advantages of the saturation algorithm 3 over strategy 2. Let us consider an operating condition where the total output voltage is composed of the first, the fifth, and the seventh harmonics, as shown in Fig. 3(a). The magnitude of $\bar{v}^S_{F1,ref}$ is lower than $V_{F,\max}$, but the voltage vectors $\bar{v}^S_{F5,req}$ and $\bar{v}^S_{F7,req}$ requested by the regulators make the total requested voltage exceed the voltage boundary. The resulting voltage vectors whose magnitude is saturated according to strategy 2 and strategy 3 are shown respectively in Fig. 3(b) and 3(c).

In strategy 2, the fifth and seventh harmonics are reduced by the same factor c' given by (26), so that the output voltage $\bar{v}^S_{F,ref}$ is brought inside the voltage limit imposed by $V_{F,\max}$, while the fundamental harmonic is kept constant. Conversely, strategy 3 reduces only the harmonic components that tend to increase the magnitude of the total output voltage. According to (29) with k=7, $\bar{v}^S_{F7,req}$ in Fig. 3(a) tends to push the total output voltage inside the voltage boundary, and its magnitude is consequently preserved. As a result, the reduction in the magnitude of the fifth harmonic necessary to comply with the voltage limit has to be less significant than the one applied by strategy 2.

Fig. 4 plots the magnitude of coefficients c_5 and c_7, calculated by dividing the fifth and the seventh voltage harmonics by the corresponding unconstrained regulator outputs, as functions of the phase angles ψ_5 and ψ_7 over a fundamental period. Strategy 2 is identified with a dashed blue line, while strategy 3 with a solid red line. Fig. 4(b) shows that the magnitude of the 7th harmonic is not affected by strategy 3, thus ensuring a more considerable voltage margin for the magnitude of the 5th harmonic, whose trend is depicted in Fig. 4(a). As a result, the magnitude of the output voltages according to strategy 3 is always greater than that obtained by strategy 2.

IV. Control Scheme

The control scheme shown in Fig. 5 is composed of two parts. The first one concerns the control of the fundamental component of the filter current. A PI regulator is used to keep

This article has been accepted for publication in a future issue of this journal, but has not been fully edited. Content may change prior to final publication. Citation information: DOI 10.1109/TIA.2020.2972853, IEEE Transactions on Industry Applications

the dc-link voltage at the reference value $E_{F,ref}$. Its output is the reference value $i_{Fd,ref}$ of the d-axis current i_{Fd}, which is proportional to the active power flow of the APF. Similarly, it is possible to control the reactive power exchange by the q-axis component i_{Fq} of the filter current. The reference value of the filter current vector is tracked by regulator R_1 (composed of a proportional-resonant regulator for each component), and a feed-forward signal $\bar{v}_G^S$ is added to its output to improve the dynamic performance.

A Phase-Locked Loop (PLL) is used to estimate the phase angle θ of the fundamental component of the grid voltage.

In the second part of the scheme of Fig. 5, the input error of the array of the proportional-resonant regulators R_1, R_2, …, R_n is obtained from the grid current, once its fundamental component has been extracted by a notch filter. The voltage request of each regulator is used by the saturation algorithm to allocate the available dc-link voltage to all the harmonic regulators, according to the implemented saturation strategy.

Finally, it is worth noting that all the saturation strategies are meant to operate in steady-state conditions.

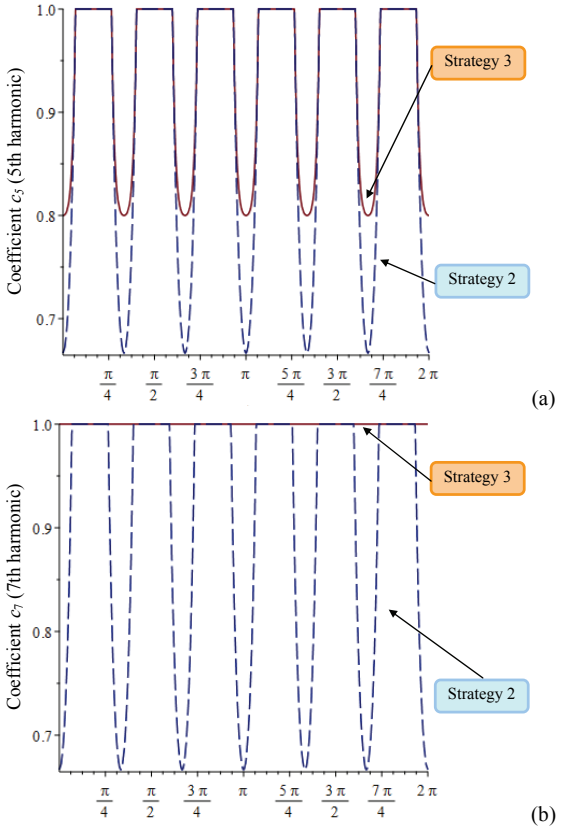

Fig.4. Magnitude of the fifth and seventh harmonic, normalized to their requested voltage. (a) Fifth harmonic. (b) Seventh harmonic.

V. Experimental Results

Some experimental results have been carried out with a laboratory prototype of a shunt APF, which is used to compensate for the highly distorted currents produced by a diode bridge feeding an RC impedance. A picture of the experimental setup is shown in Fig. 6, while the system parameters are listed in Table I. The THD of the load current is around 22%. The control system of the filter includes an array of proportional-resonant regulators to cancel the odd harmonics of the grid current from the 3rd one up to the 19th one. Fig. 7 shows that the performance of the shunt active filter is satisfactory in normal operation. As can be seen, when the APF is off, the grid current is distorted. As soon as the active filter is turned on, the grid currents become sinusoidal, and the THD reduces to about 3%.

Fig. 8 shows the behavior of the grid currents for Strategies 1, 2, and 3 when the dc-link voltage is not sufficient to generate the requested compensation voltage. The grid currents are shown in the upper part of all figures. In the lower

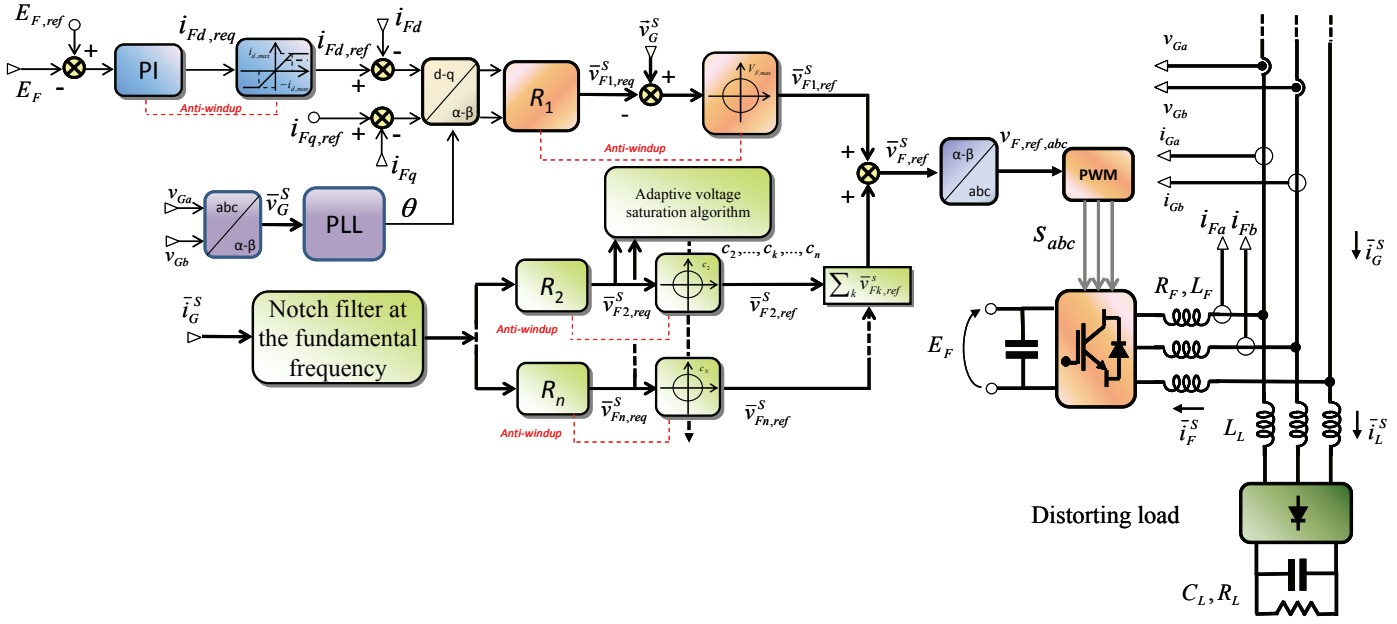

Fig.5. Proposed control scheme for the APF with adaptive saturation of the regulators.

This article has been accepted for publication in a future issue of this journal, but has not been fully edited. Content may change prior to final publication. Citation information: DOI 10.1109/TIA.2020.2972853, IEEE Transactions on Industry Applications

TABLE I – SYSTEM PARAMETERS

E_F	=	200 V_{DC}	R_F	=	50	mΩ
$V_{F,max}$	=	115 V_{peak}	L_F	=	2.36	mH
$I_{F,max}$	=	10 A_{peak}	C_L	=	0.6	mF
ω	=	2π 50 rad/s	R_L	=	60	Ω
C_F	=	2.2 mF	L_L	=	2.36	mH

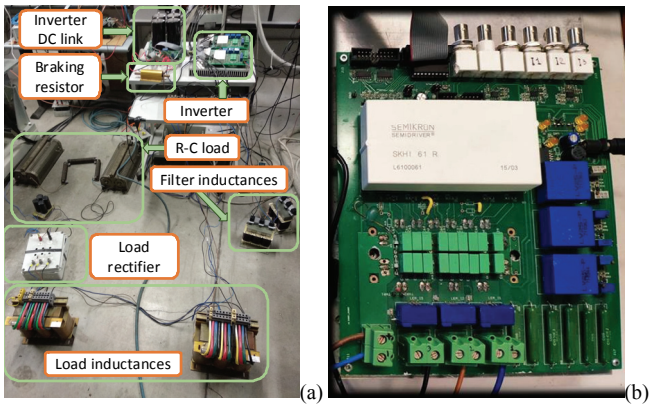

Fig.6. Photos of the experimental setup. Overview (a) and details of the power inverter (b).

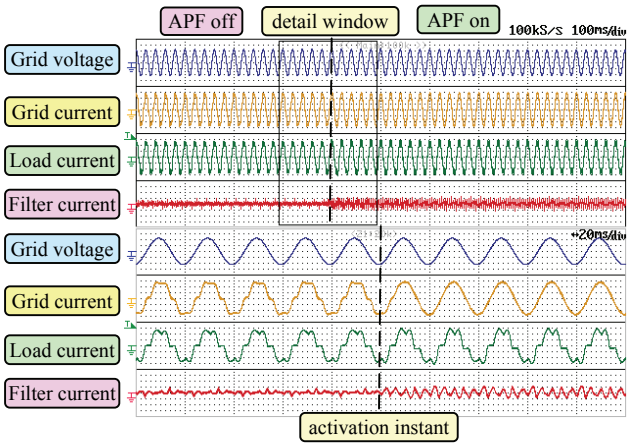

Fig.7. Waveforms of the grid currents after activating the APF. Grid voltage (50 V/div), grid current (1 A/div), load current (1 A/div), filter current (1 A/div).

part, two sub-figures show the details of the current waveforms without and with voltage saturation. Initially, the APF operates in normal conditions, and the THD of the grid current is just above 3%. Afterward, a reduction of 15% in the dc-link voltage is caused to force the saturation of the voltage regulators. As can be seen, a distortion of the grid current appears. However, the effect of the reduction in the voltage level depends on the saturation strategy. Although strategy 1 ensures that the coefficient c is constant over time, the resulting current is visibly distorted, and its waveform is nearly trapezoidal. Conversely, strategy 2 and 3 exhibit better performance, and the distortion of the grid current is less perceptible. Overall, all strategies ensure the stable operation of the converter.

Fig. 9 shows the spectrum of the space vector of the grid current in different operating conditions. If the total output voltage is below the saturation threshold, the current harmonics are negligible, as shown in Fig. 9(a). Conversely, if

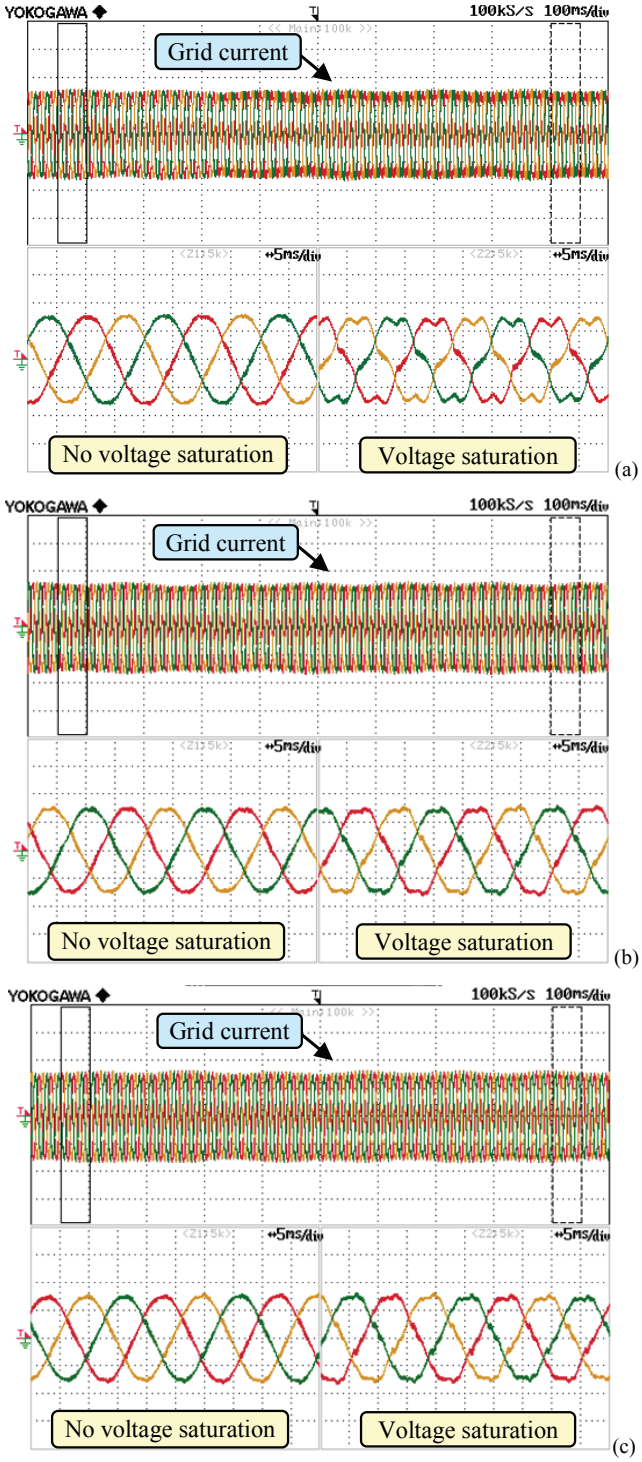

Fig.8. Waveforms of the grid current when the requested voltage is greater than the available voltage. a) Strategy 1. b) Strategy 2. c) Strategy 3. Scale: current (2 A/div).

the dc voltage becomes 85% of the rated value, some harmonics with orders -5, +7, -11, and +13 appear in the grid current. Comparing Figs. 9(b) and 9(c) leads to the conclusion that the amplitude of the harmonics generated by strategy 2 is always lower than that of the harmonics generated by strategy 1. In addition, strategy 3 seems better than strategy 2 because

This article has been accepted for publication in a future issue of this journal, but has not been fully edited. Content may change prior to final publication. Citation information: DOI 10.1109/TIA.2020.2972853, IEEE Transactions on Industry Applications

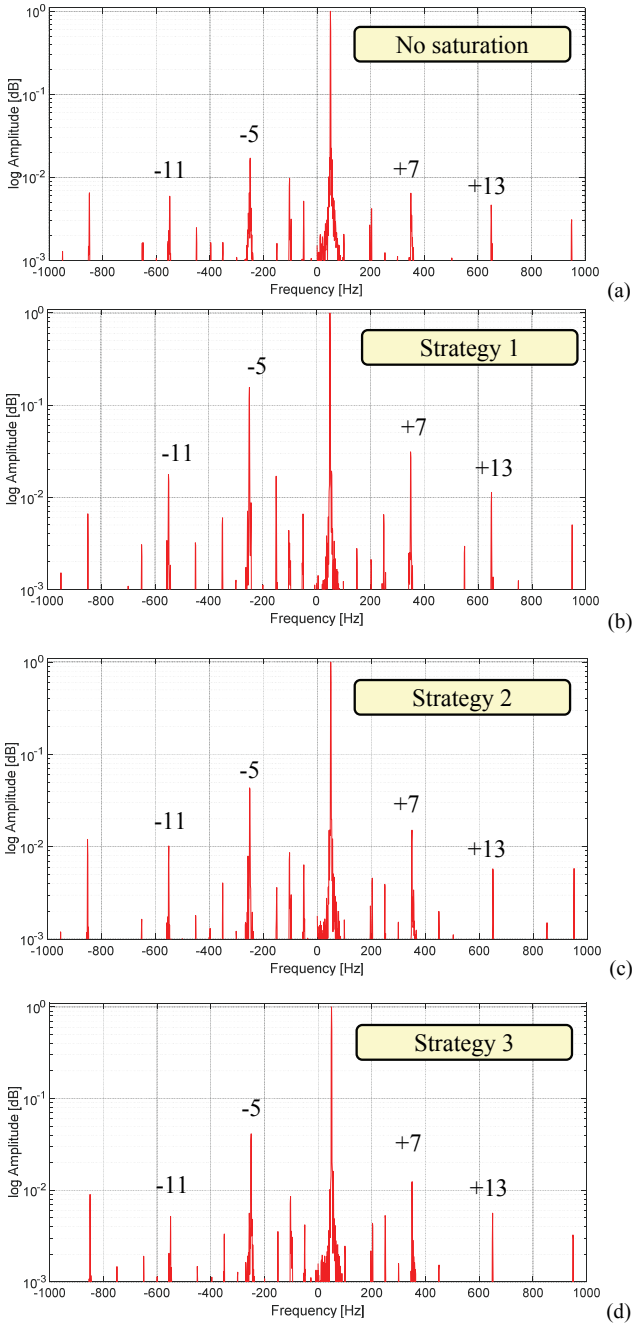

Fig.9. Spectra of the grid current for the APF without saturation of the output voltage (a) and with saturation for Strategy 1 (b), Strategy 2 (c) and Strategy 3 (d).

the harmonics with orders -5 and +7 have a smaller amplitude in Fig. 9(d).

The curves of Fig. 10 show the THD of the grid current when the dc-link voltage further decreases from 85% to 80% of the rated voltage. The THD of Strategies 2 and 3 does not change appreciably as long as the dc-link voltage is higher than 85% of the rated voltage, but below this threshold value, the performance reduction is more significant. Conversely, strategy 1 sees a linear increase in the THD as long as the dc-link voltage decreases.

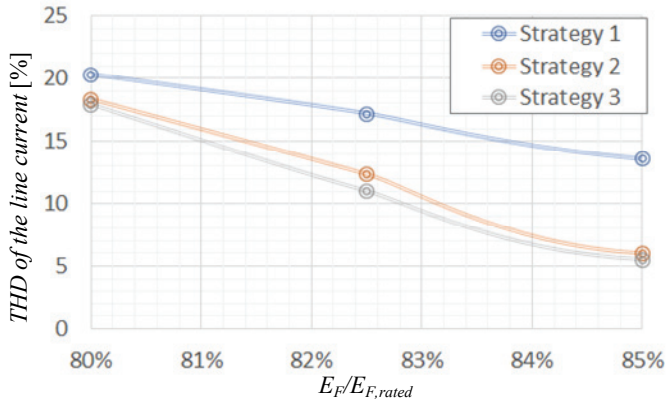

Fig. 10. THD of the grid currents when the DC-link voltage decreases causing voltage saturation.

Fig. 11 shows the output voltage of the APF for the three strategies in two different operating conditions, namely with a sufficient dc-link voltage and with an insufficient dc-link voltage to compensate for the current distortion. In the former case, depicted in Figs. 11(a)-(c), the waveform of the output voltage is similar for all strategies. Conversely, when the dc-link voltage does not allow obtaining the requested output voltage, each saturation algorithm generates a different waveform of the output voltage. Comparing Fig. 11(d) with Figs. 11(e)-(f) shows that strategy 1 produces a smoother waveform, which is less effective in canceling the high-frequency current harmonics, while the voltage loci of strategy 2 and 3 are quite similar.

Also, for each saturation strategy, the fifth and seventh harmonic components of the output voltage vector have been plotted in case of sufficient and insufficient dc-link voltage. Figs. 12(a)-(c) and Figs. 12(d)-(f) show the loci of the voltage vectors $\bar{v}^S_{F5,req}$ and $\bar{v}^S_{F5,ref}$, which are respectively the requested voltage and the reference voltage vectors at the input and output of the saturation block of regulator R_5. The first group of subfigures shows the behavior of the system with sufficient dc-link voltage, the second one with insufficient voltage. Finally, Figs 12(g)-(i) show the loci covered by the voltage vector $\bar{v}^S_{F7,ref}$ with and without sufficient voltage.

The shape of the voltage loci is elliptical because the signals contain positive and negative sequence components. As can be seen in Figs. 12(a)-(c), all strategies give similar results with a sufficient dc-link voltage, but their behavior changes when the available voltage is limited. The loci of $\bar{v}^S_{F5,ref}$ and $\bar{v}^S_{F7,ref}$ obtained with strategy 1 is generally smaller than the ones of the other strategies because strategy 1 defines the saturation constraint of each voltage harmonic according to the worst steady-state scenario. Strategy 2 saturates all the voltage harmonics proportionally to the instantaneous voltage request, while strategy 3 instantaneously constrains only the voltage components that cause the output voltage to exceed the maximum voltage. In Fig. 12(d), the loci of $\bar{v}^S_{F5,req}$ and $\bar{v}^S_{F5,ref}$ overlap with one another because the anti-windup mechanism makes these two quantities coincide at a steady

This article has been accepted for publication in a future issue of this journal, but has not been fully edited. Content may change prior to final publication. Citation information: DOI 10.1109/TIA.2020.2972853, IEEE Transactions on Industry Applications

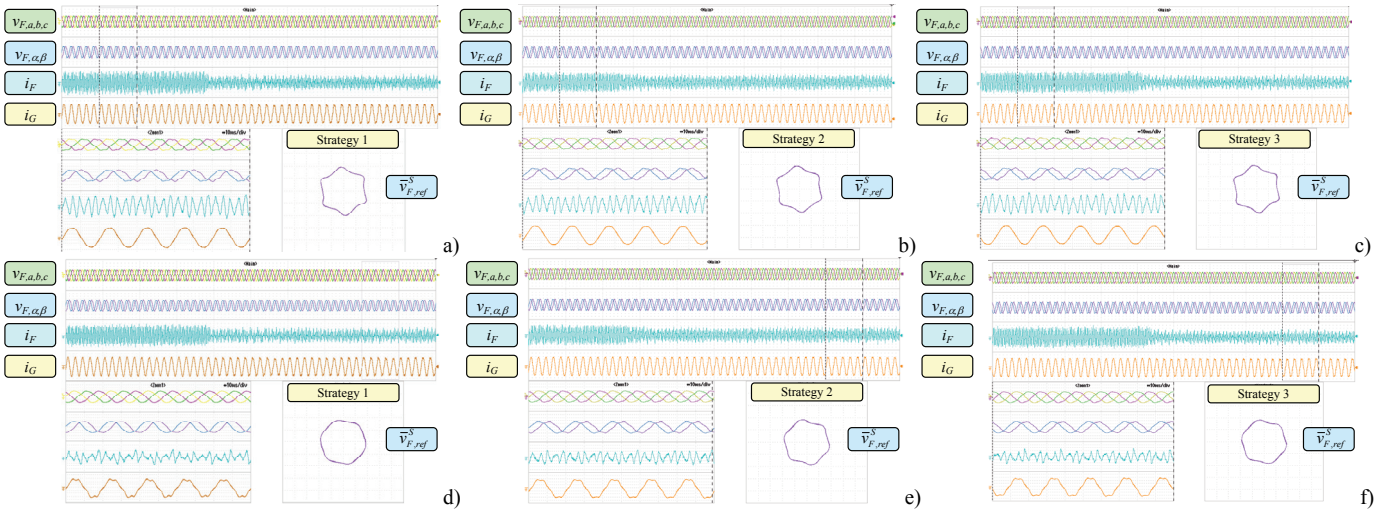

Fig.11. Behavior of the APF with Strategies 1, 2 and 3 when the dc-link voltage is sufficient (a), (b) and (c), or insufficient (d), (e) and (f). From top to bottom: inverter voltages (50 V/div), components of the inverter voltage vector, (50 V/div), inverter current (4 A/div), grid current (1 A/div). Time scale: 100 ms/div.

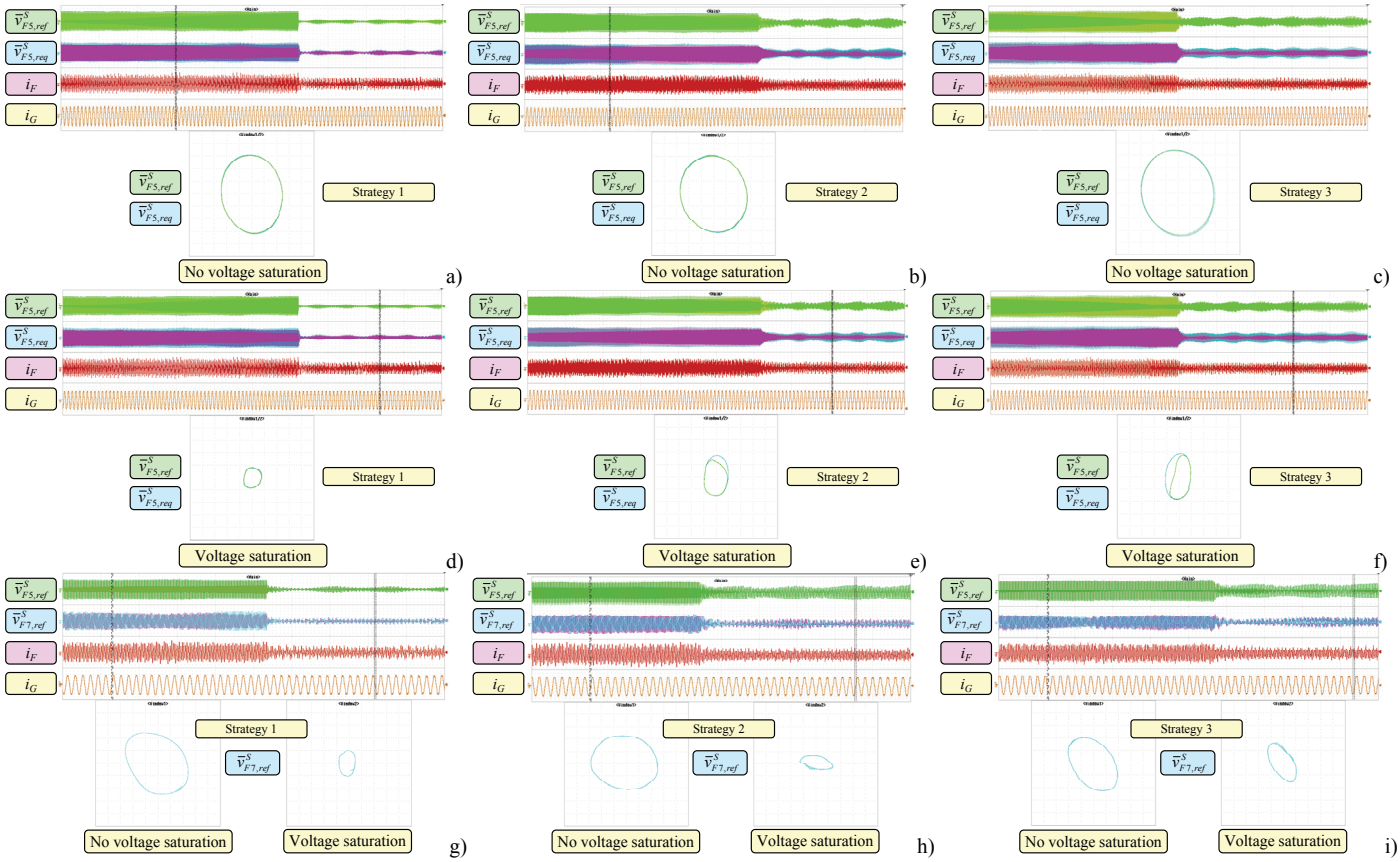

Fig.12. Behavior of the regulators of the APF with Strategies 1, 2 and 3 when the dc-link voltage with sufficient or insufficient dc-link voltage. Loci of the 5th harmonic components without saturation (a), (b), (c). Loci of the 5th harmonic components with saturation (d), (e), (f). Loci of the 7th harmonic components (g), (h), (i). Voltages of regulator R_5 (2 V/div), voltages of regulator R_7 (0.5 V/div), inverter current (4 A/div), grid current (1 A/div). Time scale 200 ms/div.

state. Conversely, in Fig. 12(e) and (h), $\bar{v}^S_{F5,ref}$ is different from $\bar{v}^S_{F5,req}$ due to the time-varying saturation boundary defined by strategy 2 and 3, which prevents the anti-windup algorithm from reaching the steady-state condition. Nevertheless, strategy 3 performs slightly better than strategy 2 and leads to a higher magnitude of the 7th voltage harmonics.

The computation times can be deduced from Fig. 13,

This article has been accepted for publication in a future issue of this journal, but has not been fully edited. Content may change prior to final publication. Citation information: DOI 10.1109/TIA.2020.2972853, IEEE Transactions on Industry Applications

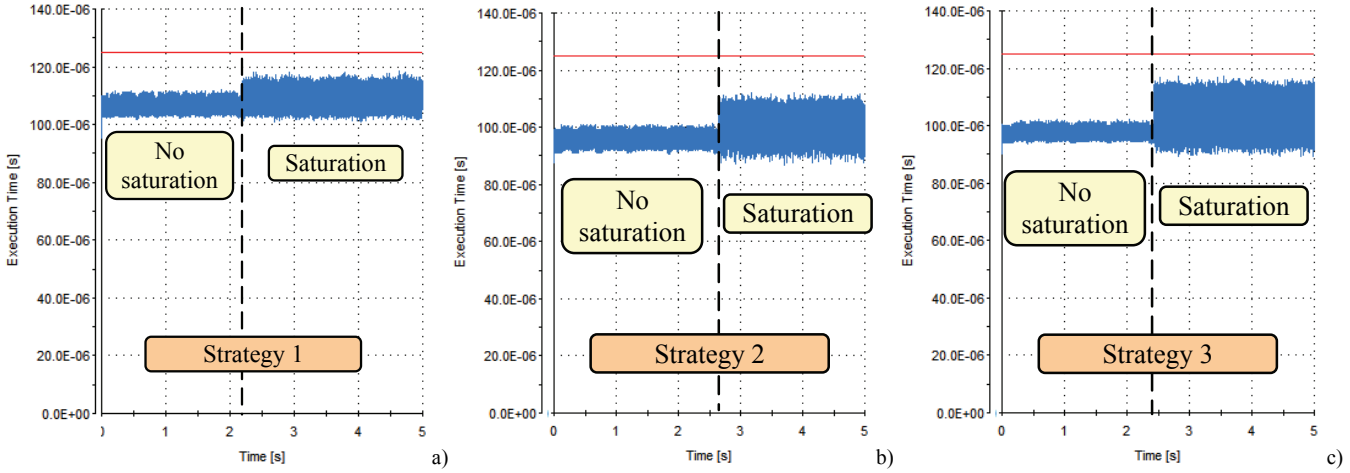

Fig.13. Computation time for Strategy 1, 2 and 3 without and with saturated voltages. The red line identifies the switching period (125 µs).

which illustrates the duration of each strategy with or without voltage saturation. The red line represents the switching period of 125 µs.

When the dc-link voltage is sufficient to generate the requested voltage vector, the computation time varies between 103 and 110 µs for strategy 1, and it fluctuates from 90 to 100 µs for strategies 2 and 3. However, in the case of voltage saturation, the maximum computation time increases from 110 µs to 115 µs for strategy 1, up to 110 µs for strategy 2 and up to 115 µs for strategy 3. This result shows that the maximum computation time is similar for all three strategies.

Strategy 3 differs from strategy 2 because it is necessary to calculate (25) for each controlled harmonic. However, (25) can be implemented as a dot product, without using trigonometric functions. Modern DSPs are specialized in "multiply and accumulate" operations, so the amount of time required to perform (25) is minimal.

VI. Conclusion

A control system for shunt APFs with selective harmonic control is presented. The paper compares three algorithms that adaptively change the voltage saturation of each resonant controller to ensure a higher voltage margin to the regulators with a higher output demand, while the performance of the fundamental controller is preserved. The experimental results confirm the stable operation of the APF and the feasibility of the adaptive algorithms. According to the experimental results, Algorithm 3 shows the best performance.

References

[1] H. Akagi, “Control strategy and site selection of a shunt active filter for damping of harmonic propagation in power distribution systems,” IEEE Trans. Power Del., vol. 12, no. 1, pp. 354–362, Jan. 1997.

[2] C. D. Schauder and S. A. Moran, “Multiple reference frame controller for active filters and power line conditioners,” U.S. Patent 5 309 353, May 3, 1994.

[3] S. Bhattacharya, A. Veltman, D.M. Divan, and R. D. Lorenz, “Flux-based active filter controller,” IEEE Trans. Ind. Appl., vol. 32, no. 3, pp. 491– 502, May/Jun. 1996.

[4] P.-T. Cheng, S. Bhattacharya, and D. M. Divan, “Experimental verification of dominant harmonic active filter for high-power applications,” IEEE Trans. Ind. Appl., vol. 36, no. 2, pp. 567–577, Mar./Apr. 2000.

[5] L.Malesani, P. Mattavelli, and S. Buso, “Robust dead-beat current control for PWM rectifiers and active filters,” IEEE Trans. Ind. Appl., vol. 35, no. 3, pp. 613–620, May/Jun. 1999.

[6] S. Buso, L. Malesani, and P. Mattavelli, “Comparison of current control techniques for active filters applications,” IEEE Trans. Ind. Electron., vol. 45, no. 5, pp. 722–729, Oct. 1998.

[7] S. Buso, S. Fasolo, L. Malesani, and P. Mattavelli, “A dead-beat adaptive hysteresis current control,” IEEE Trans. Ind. Appl., vol. 36, no. 4, pp. 1174–1180, Jul./Aug. 2000.

[8] P. Mattavelli and F. P. Marafao, “Repetitive-based control for selective harmonic compensation in active power filters,” IEEE Trans. Ind. Electron., vol. 51, no. 5, pp. 1018–1024, Oct. 2004.

[9] M. J. Newman, D. N. Zmood, and D. G. Holmes, “Stationary frame harmonic reference generation for active filter systems,” IEEE Trans. Ind. Appl., vol. 38, no. 6, pp. 1591–1599, Nov./Dec. 2002.

[10] X. Yuan, W. Merk, H. Stemmler, and J. Allmeling, “Stationary-frame generalized integrators for current control of active power filters with zero steady-state error for current harmonics of concern under unbalanced and distorted operating conditions,” IEEE Trans. Ind. Appl., vol. 38, no. 2, pp. 523–532, Mar./Apr. 2002.

[11] M. Bojrup, P. Karlsson, M. Alakula, and L. Gertmar, “A multiple rotating integrator controller for active filters,” in Proc. EPE Conf., 1999. CD-ROM.

[12] C. Lascu, L. Asiminoaei, I. Boldea, F. Blaabjerg, “Frequency response analysis of current controllers for selective harmonic compensation in active power filters,” IEEE Trans. Ind. Elect., vol. 56, no. 2, pp. 337-347, Feb. 2009.

[13] P. Mattavelli, “A closed-loop selective harmonic compensation for active filters,” IEEE Trans. Ind. Appl., vol. 37, no. 1, pp. 81–89, Jan./Feb. 2001.

[14] A. Amerise, M. Mengoni, L. Zarri, A. Tani, G. Serra, D. Casadei, “Control system for shunt active power filters with adaptive voltage saturation,” IEEE Energy Conversion Congress and Expo, Cincinnati, US, Sept. 30- Oct. 5, 2017, pp. 682-687.

[15] M. Rizo, M. Liserre, E. J. Bueno, F. J. Rodríguez, A. Rodríguez, “Distortion-free saturators for power converters under unbalanced conditions," EEE Trans. Pow. Electron., vol. 30, no. 6, pp. 3364-3375, June 2015.

[16] L. Harnefors, A. G. Yepes, A. Vidal, J. Doval-Gandoy, “Multifrequency current control with distortion-free saturation,” IEEE Journal of Emerging and Selected Topics in Power Electronics, vol. 4, no. 1, pp. 37-46, March 2016.

[17] J. Moriano, M. Rizo, E. Bueno, J. R. Sendra, R. Mateos, “Distortion-free instantaneous multifrequency saturator for THD current reduction,” IEEE Transactions on Industrial Electronics, vol. 66, no. 7, pp. 5310-5320, July 2019.

[18] A. Amerise, M. Mengoni, G. Rizzoli, L. Zarri, A. Tani, D. Casadei, "Adaptive Voltage Saturation Algorithms for Selective Harmonic Control in Shunt Active Power Filters," IEEE ECCE 2018, Portland, US, September 23-27, 2018, pp. 5692-5698.

[19] A. Lidozzi, M. Di Benedetto, S. Bifaretti, L. Solero, F. Crescimbini, "Resonant controllers with three degrees of freedom for AC power electronic converters," IEEE Trans. Ind. Appl., vol. 51, no. 6, pp. 4595, 4604, Nov./Dec. 2015.

Albino Amerise received the M.Sc. degree (with honors) and the PhD degree in electrical engineering respectively in 2015 and 2018 from the University of Bologna, Bologna, Italy. In 2019 he was a research assistant the Department of Electric, Electronic and Information Engineering "G. Marconi", University of Bologna. He is currently with Magneti Marelli SpA. His research interests include vector control of induction machines and grid-connected converters.

Michele Mengoni was born in Forlì, Italy. He received the M. Sc. and Ph. D. degrees in Electrical Engineering from the University of Bologna, Bologna, Italy, in 2006 and 2010, respectively. He is currently a Senior Assistant Professor with the Department of Electric, Electronic and Information Engineering "G. Marconi", University of Bologna. His research interests include design, analysis, and control of three phase electric machines, multiphase drives, and ac/ac matrix converters.

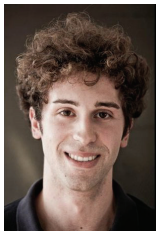

Gabriele Rizzoli received the M.Sc and Ph.D. degree in Electrical Engineering, respectively in 2012 and 2016, from the University of Bologna, Bologna, Italy. In 2015 he was a visiting student at Virginiatech (CPES), Blacksburg, Virginia, United States of America. He is currently a research assistant at the Department of Electrical, Electronic and Information Engineering "G. Marconi" of the University of Bologna. His research interests include the design of electrical machines, the development and control of high-efficient power converters for automotive and renewable energy applications.

Luca Zarri (M'05-SM'12) received the M. Sc. and Ph.D. degree in Electrical Engineering from the University of Bologna, Bologna, Italy, in 1998 and 2007, respectively. Currently, he is an Associate Professor with the Department of Electrical, Electronic, and Information Engineering "Guglielmo Marconi", University of Bologna. He has authored or coauthored more than 150 scientific papers. His research activity concerns the control of power converters and electric drives. He is a senior member of the IEEE Industry Applications, IEEE Power Electronics and IEEE Industrial Electronics Societies.

Angelo Tani received the M. Sc. degree in Electrical Engineering, with honors, from the University of Bologna, Bologna, Italy, in 1988. Currently he is a Full Professor of power electronics, electrical machines and drives with the Department of Electric, Electronic and Information Engineering, University of Bologna. He has authored more than 180 papers published in technical journals and conference proceedings. His current activities include multiphase and three phase electric drives, diagnostic techniques for electric machines, and active filters.

Domenico Casadei (F'15-SM'04) received the M. Sc. in Electrical Engineering (with honors) from the University of Bologna, Italy, in 1974. He is Full Professor of Electrical Drives with the Department of Electrical, Electronic, and Information Engineering "Guglielmo Marconi", University of Bologna. He is author and co-author of more than 250 scientific papers, published in technical journals and conference proceedings. His research areas are vector control of AC drives and diagnosis of electrical machines. He is a member of the IEEE Industrial Electronics Society, IEEE Power Electronics Society and European Power Electronics Society. He has been elevated to the grade of IEEE Fellow for contributions to direct torque control and matrix converters in electric drives.